Compression mechanisms in quasimolecular XI3 (X = As, Sb, Bi) solids

Compression mechanisms in quasimolecular XI_3 (X=As,Sb,Bi) solids

H. C. Hsueh and Roger K. Chen
Department of Physics, Tamkang University, Tamsui, Taiwan 25137, Republic of China

H. Vass, S. J. Clark, G. J. Ackland, W. C-K. Poon, and J. Crain
Department of Physics and Astronomy, The University of Edinburgh, Edinburgh, EH9 3JZ, Scotland, United Kingdom
(Received 13 November 1997; revised manuscript received 29 May 1998)

We explore the structural, vibrational, and electronic properties of a prototypical family of quasimolecular layered solid of the type XI_3 where (X=As,Sb,Bi) under compression. We use a combination of angle-dispersive powder x-ray diffraction and Raman spectroscopy to study the structural and vibrational response to pressure. We also perform first-principles density functional pseudopotential calculations using both the local density approximation and gradient-corrected techniques for the description of electron exchange and correlation to further examine the electronic properties under pressure. We find that an unusual nonmonotonic variation of the symmetric X-I stretch frequency can be unambiguously attributed to the formation of intermolecular bonds and that compression results in a sequence of transitions from hexagonal molecular to hexagonal layered to monoclinic. The pressure dependence of the ambient pressure hexagonal structure is given as a full structural determination of the high-pressure phase. The structural and vibrational response (including the complex pressure dependence of the bond-stretch frequency) is well accounted for by quantum mechanical simulation. We further find that gradient corrections are necessary for an appropriate description of equilibrium structure, bonding, vibrational properties, and compression mechanisms and that the local density approximation appears to fail badly. [S0163-1829(98)07445-1]

I. INTRODUCTION

The response to compression of highly anisotropic materials such as layered and molecular solids has long been recognized as an important probe of structure and bonding in these important systems.[1–3] Unlike isotropic tetrahedrally bonded semiconductors or metals where pressure effects have been studied in great detail, cohesion in layered or molecular materials occurs through forces of very different strengths. This manifests itself in a relatively large disparity between interlayer, intralayer, or molecular distances and an associated separation in vibrational frequencies.[2] In layered systems, for example, the ambient pressure vibrational spectrum contains very low-frequency interlayer modes arising from the relative motion of rigid layers. In general, it is expected that pressure will have the effect of preferentially enhancing weak interactions thereby decreasing the degree of anisotropy.

Historically however, it has proved difficult to study the structural, electronic, and dynamic properties of these materials in detail under pressure primarily because the crystal structures tend to be very complex, having crystal symmetries lower than tetragonal and several free internal parameters. The limitations of conventional x-ray diffraction studies from small samples contained in diamond anvil pressure cells have, until recently, precluded investigations into the detailed structural evolution under pressure. Moreover the structural complexity of these materials has also meant that they have been relatively unexplored by predictive, parameter-free computer simulations.

With the development and subsequent refinement of high-pressure angle-dispersive powder diffraction methods (using area detectors[4]), high-resolution optical spectroscopic techniques,[5] and advanced algorithms for efficient electronic structure calculations,[6] it has recently become possible to examine structure and bonding under hydrostatic conditions in complex anisotropic systems at new levels of detail. The first detailed studies of the influence of pressure in layered materials have been reported for isostructural GeS (Refs. 5,7) and GeSe (Ref. 8) for which it was demonstrated that the rigid layer approximation fails at even modest pressures and that substantial mode admixture occurs. This breakdown of quasi-two-dimensional character in the vibrational behavior occurred when the materials were still structurally anisotropic.

Here we study the structural, electronic, and vibrational response to compression of a prototypical family of quasimolecular solids of the type XI_3 (where X=As,Sb,Bi). In some members of this family of isostructural compounds, two-dimensional layering coexists with well-defined molecular units. There are therefore a wide range of interactions present in these systems each of which may exhibit different responses to density variation thereby giving rise to competing interactions, complex compression mechanisms, and structural instabilities. A preliminary account of pressure-induced electron transfer effects in these systems has been recently reported,[9] however, there remain many unresolved issues concerning the bonding and compression mechanisms in these materials.

The purpose of this paper is therefore to (1) explore pressure-induced structural, electronic, and vibrational effects in anisotropic solids, (2) interpret unusual features ob-

served in both the high- and low-frequency regions of the vibrational spectrum, (3) identify the structures of new high-density polymorphs of these materials and explain the observed structural phase transitions in terms of simple models, and (4) determine the accuracy with which parameter-free computer simulation methods can predict the complex structure, compression mechanisms, and dynamical properties in anisotropic systems and thereby to provide insight into the nature of bonding in these complex molecular solids.

To this end we use a combination of synchrotron x-ray diffraction using an image plate area detector, high-resolution Raman scattering, and *ab initio* computer simulation using full structural relaxation.

The paper is organized as follows. In the next section we outline the experimental methods and procedures followed to obtain structural and dynamical information under pressure. We also outline relevant aspects of the computational modeling. We then present the combined results of the experimental measurements and theoretical calculations and discuss the interpretation of the findings.

II. METHODS

A. Angle-dispersive powder x-ray diffraction

Samples of all three materials were obtained from ALFA products and used without further purification. The samples were ground to a fine powder to minimize the effects of preferred orientation and loaded into a diamond anvil pressure cell without a pressure-transmitting medium. The usual 4:1 methanol:ethanol solution was not used for these materials because they are moisture sensitive. Pressure was monitored using the ruby fluorescence scale and the widths of the fluorescence lines were taken as a qualitative indication of the degree of hydrostaticity in the sample chamber. The ruby fluorescence signal remained a well-defined doublet over all pressure ranges and we interpret this to mean that the influence of nonhydrostatic effects is negligibly small compared to the hydrostatic pressure. All diffraction profiles were recorded at room temperature.

Synchrotron x rays at a wavelength of 0.4447 Å from station 9.1 of the Daresbury Laboratory Synchrotron radiation facility were used in conjunction with an image plate x-ray area detector to record powder diffraction profiles. Typical exposure times were 4 h. Integration of the two-dimensional powder images was performed using the software package PLATYPUS[4] which converted the images to standard profiles. Subsequent data analysis and structural refinement was performed using the GSAS suite of Reitveld refinement programs.

B. Vibrational Raman spectroscopy

Sample sources and preparation for vibrational spectroscopic measurements were the same as for the diffraction measurements. Raman spectra were collected from a dry-loaded diamond anvil pressure cell in backscattering geometry using the 6764 Å line of a Kr^+ ion laser as the excitation source. A Spex triple-grating scanning spectrometer was used for data collection. Spectral resolution was 1.5 cm^{-1} and count times were approximately 10 sec.

Low-temperature data were collected using a CTI Cryogenics closed-cycle cryostat and a Lakeshore Cryogenics temperature controller. The sample was firmly affixed to a copper backing plate which made thermal contact with the sample. Temperature control was better than 0.1 K. The scattering geometry and instrumental resolution was identical to the high-pressure arrangement.

C. *Ab initio* density functional calculations

1. Electronic properties and structure optimization

Density functional[10] pseudopotential calculations were carried out on AsI_3 using an adaptation of the original CASTEP code[6] modified to perform full structural relaxation under the influence of arbitrary stresses and for symmetry-adapted normal mode and frequency calculations. Here the equilibrium geometry was determined by relaxation under the influence of Hellmann Feynman forces[11] and stresses using the methods described in Refs. 5,7. Nonlocal pseudopotentials were generated in the Kleinman-Bylander form using the Q_c tuning method.[12,13] The energy cutoff of 320 eV was used for the expansion of the plane wave basis set. Structural relaxation proceeded until no force component exceeded 0.002 eV/Å where the calculated total energies were converged to better than 0.1 MeV/cell. The Brillouin zone sampling of AsI_3 was performed using six special k points which correspond to the $3\times3\times3$ Monkhorst-Pack[14] k-point grid appropriate for the symmetry of the rhombohedral unit cell having space group $C_{3i}^2(R\bar{3})$. To investigate the subtle structural and electronic properties of AsI_3 with highly molecular character at ambient pressure, both the local density approximation (LDA)[15] and the general-gradient approximation (GGA)[16] were employed to describe the electron exchange-correlation interactions.

2. Vibrational properties

For calculations of vibrational mode frequencies, a small set of displacements was made giving rise to harmonic restoring forces on all other atoms in the unit cell. Exploitation of space group symmetry allowed for the construction of the full dynamical matrix which, when diagonalized, yields vibrational mode frequencies and associated eigenvectors. The details of phonon frequency calculations can be found elsewhere.[7,17] In this work we consider displacements in a single unit cell which therefore generate only Brillouin zone center modes. The parallel version of our code (CETEP) implemented on a Cray T3D was used for all the first-principle zone-center phonon calculations. To minimize the effects of numerical noise in the vibrational calculations we make both positive and negative displacements of the atoms from their equilibrium positions and average the resulting restoring forces. In these calculations a typical displacement is 0.005 in fractional coordinates. Since the distorted structures correspond to a lower symmetry configuration the number of special sampling points was increased to 14.

III. RESULTS

A. Ambient pressure structures of XI_3 quasimolecular compounds

The ambient pressure structures of AsI_3 and SbI_3 have been examined previously using single crystal x-ray

TABLE I. Calculated and observed lattice constants (in Å), internal parameters (in fractional coordinate) with e.s.d.'s in parentheses, bondlength b (in Å), nearest-unbonded length b_n (in Å), and bond angle bg (in degrees) for XI_3 (X=As,Sb,Bi) under ambient condition.

Compound	a	c	z_X	x_I	y_I	z_I	b	b_n	bg
AsI_3 [a]	7.208	21.436	0.1985	0.3485	0.3333	0.0822	2.556	3.50	102
AsI_3 [b]	7.193(2)	21.372(7)	0.80451(8)	0.31750(9)	−0.00662(9)	0.74749(3)	2.591(1)	3.467(2)	99.67(5)
AsI_3 [c]	7.208(2)	21.415(3)	0.2001(1)	0.3447(7)	0.3187(7)	0.0772(6)	2.56(7)	3.55(9)	99.9(3)
AsI_3 [d]	7.248	21.547	0.1902	0.3522	0.3259	0.0858	2.57	3.34	99
AsI_3 [e]	7.031	20.223	0.1686	0.3357	0.3158	0.0864	2.77	2.83	90
SbI_3 [a]	7.48	20.90	0.1820	0.3415	0.3395	0.0805	2.868	3.32	99
SbI_3 [c]	7.505(1)	20.966(7)	0.1812(1)	0.3397(3)	0.3233(2)	0.0816(4)	2.83(4)	3.24(9)	95.2(2)
BiI_3 [a]	7.516	20.718	0.1667	0.3415	0.3395	0.0805	3.1	3.1	89
BiI_3 [c]	7.526(7)	20.731(6)	0.1693(1)	0.3322(4)	0.3146(3)	0.0797(3)	3.01(0)	3.06(4)	89.6(1)

[a]Reference 18.
[b]Reference 19.
[c]Reference 9.
[d]GGA calculation.
[e]LDA calculation.

diffraction.[18] The results of these measurements along with our experimental values (as determined by powder x-ray diffraction in a diamond cell) are shown in Table I. It is clear that our x-ray results are comparable to those of the earlier structural studies. An example of the least squares fit to the powder diffraction data is shown in Fig. 1.

All three members of the tri-iodide family have crystallographically equivalent structures [rhombohedral with space group $C_{3i}^2(R\bar{3})$ (Refs. 9,18,19)] though it has been found that the molecular character of the XI_3 units differs as a result of internal degrees of freedom. Specifically, in the AsI_3 compound, the molecular units are well preserved. There is clear threefold coordination and the molecular geometry in the solid is close to that of gas phase AsI_3.[18] The molecular character is lost in BiI_3 which exhibits near-perfect sixfold coordination of the metal. The Sb material is an intermediate case. In the three materials there is an iodine sublattice in which the iodine atoms exist in well-defined planar double layers as shown in Fig. 2. As is evident from the figure, the atoms in the individual layers are not close packed. The group-V atoms reside in the interstices separating layers.

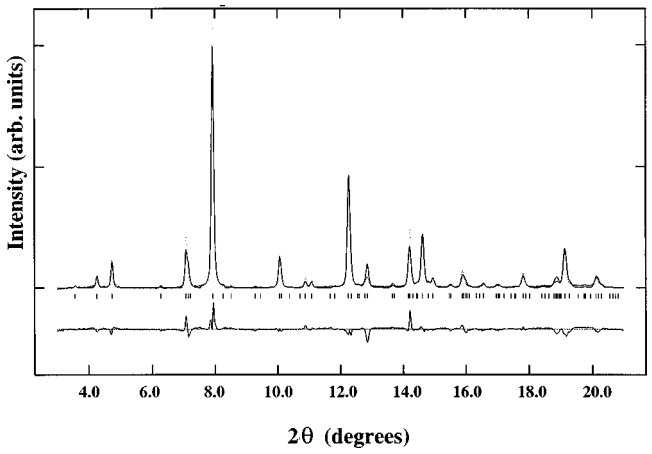

FIG. 1. Rietveld refinement of powder pattern of AsI_3 obtained at ambient pressure. The observed data are denoted as dots and the symbol | represents the calculated reflection. The solid line is the calculated profile whereas the difference between the calculation and observation is shown as another solid line in the lower panel. The corresponding refinement reliability factor $R_{wp}(\%)$ is 4.07.

The electronic origin of this structural trend can be interpreted in terms of the different types of bonding available for the metal atom. For example, the valence electron configuration of group-V metals is ns^2np^3. This permits, in principle, the formation of tri-iodides having either ionic or covalent character. In the ionic case, s electrons do not participate and the three p electrons are donated to give X^{3+} cations, each surrounded octahedrally by six I^- anions. The pure covalent case is defined by complete sp^3 hybridization, with three covalent metal-iodine bonds and one lone pair associated with each metal. This gives distinct XI_3 molecules in the solid state. According to this description, the ionic case applies for the Bi-containing compound and covalent bonding is favored for AsI_3.

Density functional calculations have been applied to study the ambient pressure structure of AsI_3 and the results are also shown in Table I which includes experimental data for comparison. It is evident that the ground state structures are sensitive to the description of the electron exchange and correlation potential. In calculations using the local density approximation, the molecular units are not preserved and intermolecular bonding is found. A comparison between the calculated electronic charge distributions is shown in Fig. 3.

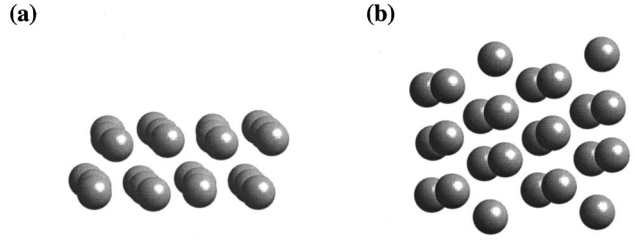

FIG. 2. Illustration of the Iodine sublattice at ambient pressure as viewed parallel (a) and perpendicular (b) to the double layers. It shows the highly symmetric arrangement of the atoms

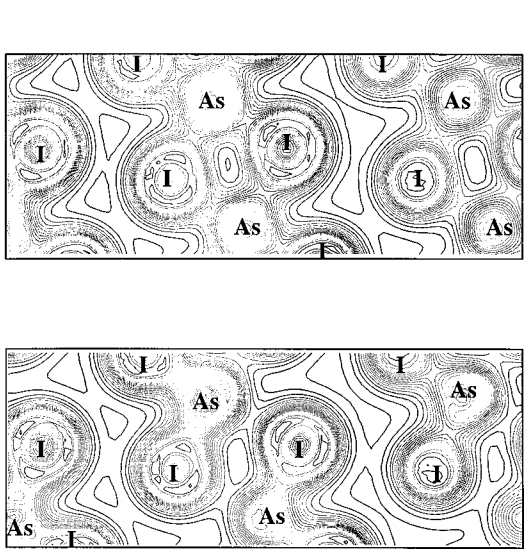

FIG. 3. Contour plot of the valence electronic charge distribution for AsI_3 displayed in a (012) plane as calculated using the density functional pseudopotential method as described in the text. Calculations have been performed using both the local density approximation (LDA) (a) and the generalized-gradient approximation (GGA) (b). It is evident that the LDA method leads to a greater degree of intermolecular covalent bonding than does the GGA.

The coordination is predicted to be quasi-sixfold which is not in accord with x-ray structural results on either single crystal or powdered samples at ambient pressure. The calculated unit cell volume using the LDA is 144.3 $Å^3$/molecule at ambient pressure for AsI_3. This corresponds to a 10% underestimate of the experimental value of approximately 160 $Å^3$/molecule as obtained from powder and single crystal diffraction experiments. The use of the generalized gradient approach provides a qualitatively different description of the bonding. Specifically, the AsI_3 molecular units are found to be preserved in the GGA calculations. The structural origin of this difference (as seen in Table I) is due to a substantially larger value of the equilibrium intramolecular I-As-I bond angle (by approximately 10° in the GGA calculation). Furthermore it is seen that the separation between atoms on adjacent molecules is also larger by about (0.5 Å) according to the GGA result. This value is similar to that observed in the diffraction experiments. The overall molecular volume as determined by GGA calculations is also in far better accord (within 1%) with the experimental value and is slightly overestimated.

The tendency of the LDA to underestimate lattice parameters has been reported previously but in general such studies have been confined to isotropic systems.[20] Recent investigations of the ambient pressure structure of tellurium and selenium have revealed that LDA introduces an additional effective pressure to the system rather than a uniform volume underestimate.[21,22] This does not appear to be the case for these anisotropic materials where the discrepancy is not accounted for by assigning the LDA-calculated structure to that found experimentally for the $R\bar{3}$ phase at hydrostatically compressed volumes. As shown in the table, the calculated value of the positional parameter $z(\mathrm{As})$ is close to that found experimentally at a pressure of about 79 kbar, however, the calculated lattice constants a and c, are much larger than the ones observed at that pressure. In other words, although the volume is clearly underestimated in the LDA calculation, the compressed structure is not what is expected if an effective hydrostatic pressure were present. We will investigate this point in more detail in a later section in connection with vibrational properties.

B. Structural response to pressure and phase transitions

1. Compression mechanism of the rhombohedral structure

The evolution of the powder diffraction patterns for the three materials is shown in Fig. 4. The example of high-

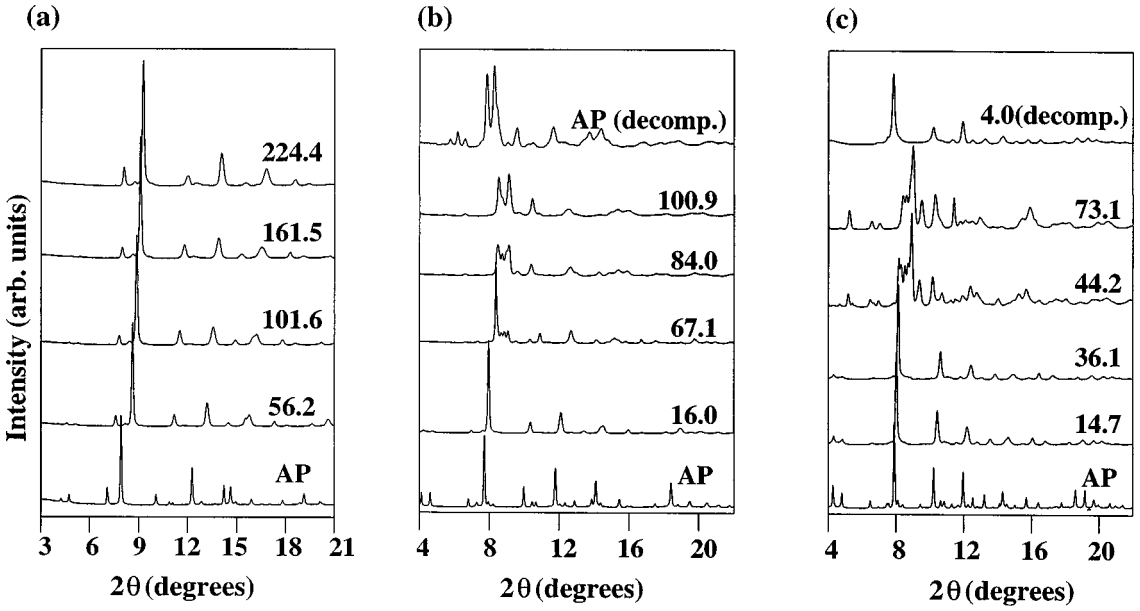

FIG. 4. Evolution of powder diffraction patterns for AsI_3 (a), SbI_3 (b), and BiI_3 (c) as a function of increasing pressure. The strength of pressure is indicated in a unit of kbar. The decompressional measurement of the Sb and Bi compound (see in the text) is also shown in (b) and (c), respectively (denoted as decomp.).

TABLE II. Lattice constants (in Å) and internal parameters (in fractional coordinate) obtained from Rietveld refinement for XI_3 (X=As,Sb,Bi) at high pressure (kbar). The refinement reliability factors for R_{wp} are also provided. (e.s.d.'s are shown in parentheses).

Compound	Pressure	a	c	z_X	x_I	y_I	z_I	R_{wp}(%)
AsI_3	101.6	6.530(6)	18.121(5)	0.1676(1)	0.3306(2)	0.3482(8)	0.0739(2)	4.7
SbI_3	16.0	7.302(7)	20.016(8)	0.1688(8)	0.3372(2)	0.3456(4)	0.0768(2)	8.8
BiI_3	14.7	7.327(5)	20.029(1)	0.1680(4)	0.3291(7)	0.3328(4)	0.0758(4)	9.0

pressure structural parameters from Rietveld refinement for all three tri-iodides are listed in Table II. In the rhombohedral phase of all three compounds, we find that the effect of pressure is to reduce the layer separation as expected but also to twist the molecular units. The effect on the structure is illustrated in Fig. 5. Under pressure the iodine atoms adopt increasingly staggered positions within a layer. These structural changes do not correspond to a lowering of symmetry as they remain consistent with the $R\bar{3}$ spacegroup symmetry (see discussion on ambient pressure structure in the next section).

For AsI_3, the experimental bulk modulus as obtained from a fit to the third-order Birch-Murnaghan equation of state is 624.7 kbar whereas the calculated value (using gradient corrections) is 552 kbar. The difference between observed and calculated values is attributed to the dependence of bond strengths on temperature which is most clearly reflected in the vibrational frequencies. Further discussion is deferred to the section on vibrational properties. The observed and calculated first pressure derivative of the bulk modulus is $B_0'=9.55$ and 9.14, respectively and the molecular volumes are 160.60 Å^3/molecule and 163.38 Å^3/molecule, respectively. In the cases of AsI_3 and SbI_3 the effect of pressure is to reduce intermolecular separation resulting in the formation of intermolecular bonds. This gives rise to sixfold coordination of the metal atom. The Bi compound is already sixfold coordinated at ambient pressure. Based on the structural evidence, the effect of pressure is similar to the chemical effect caused by substitution of heavier group-V species.

A full comparison of the observed and calculated structural compression mechanism (using generalized gradient corrections) is shown in Fig. 6. It is evident that the complex response to compression is generally very well accounted for in the simulations. This is evidenced by the very good agreement between observed and simulated results for the a and c lattice parameters and the positional parameters z_{As}. In fact, agreement to within experimental error is obtained in most of these cases over the full pressure range of measurement. There are small quantitative discrepancies for the other positional parameters but the trends in the pressure-induced response is in accord with the experimentally observed findings.

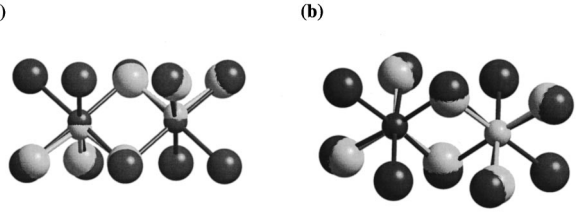

FIG. 5. An illustration of the structural response to compression showing the twisting of SbI_3 molecular units. The lighter and darker spheres correspond to the atomic positions at ambient pressure and 54 kbar, respectively. The small sphere stands for the Sb atom and large one for the I atom.

2. Rhombohedral to monoclinic transition

The evolution of the powder profile with increasing pressure reveals a clear structural transformation in both the Bi and Sb compounds which occurs beyond 70 and 40 kbar, respectively. No structural transition was found in the As material up to the maximum pressure attainable in our cell though such a transition is likely at higher pressure. The high-pressure phases of both the Sb and Bi compounds were indexed on a monoclinic unit cell in the space group $P\ 2_1/c$, C_{2h}^5. This high-pressure structure is similar to the greenish-yellow monoclinic modification of SbI_3 which was found by Pohl *et al.*[23] from single crystal x-ray diffraction under ambient condition.

The high-pressure phase of the Sb material was found to have lattice parameters $a=6.636(4)$ Å, $b=9.375(2)$ Å, $c=8.165(1)$ Å with $\beta=108.41(2)°$ at 101 kbar. The internal structure contains four molecules per unit cell and all atoms in the four-atom basis reside on completely free positions. The refined values of these internal atomic coordinates at 101 kbar are given in Table III. A least squares (Rietveld) fit to the powder pattern recorded for SbI_3 from which these parameters were obtained is shown in Fig. 7(a). The refinement of BiI_3 at 73.1 kbar also shows a similar monoclinic structure (possible space group is $P\ 2_1/c$) with lattice parameters $a=6.728(1)$ Å, $b=9.565(5)$ Å, $c=8.106(8)$ Å, and $\beta=107.56(2)°$.

Schematic illustrations of the high-pressure phase of SbI_3 based on these structural parameters are shown in Figs. 7(b) and 7(c). It is evident that the sixfold coordination of the metal atom is substantially distorted in this low-symmetry polymorph. In fact, the coordination can be described at best as quasi-sixfold coordinated as the bond lengths in the closest coordination shell for the group-V atoms vary by 10% at 90 kbar. It is perhaps more accurate therefore to describe the high-pressure phase as a mixed coordination compound.[24] The transition to the monoclinic phase further disrupts the layer structure of the iodine sublattice substantially as shown in Fig. 8. Specifically the layers are found to buckle in the high-pressure modification. In the case of SbI_3 the high-pressure monoclinic phase is found to be far less compressible than the rhombohedral phase. Specifically the bulk

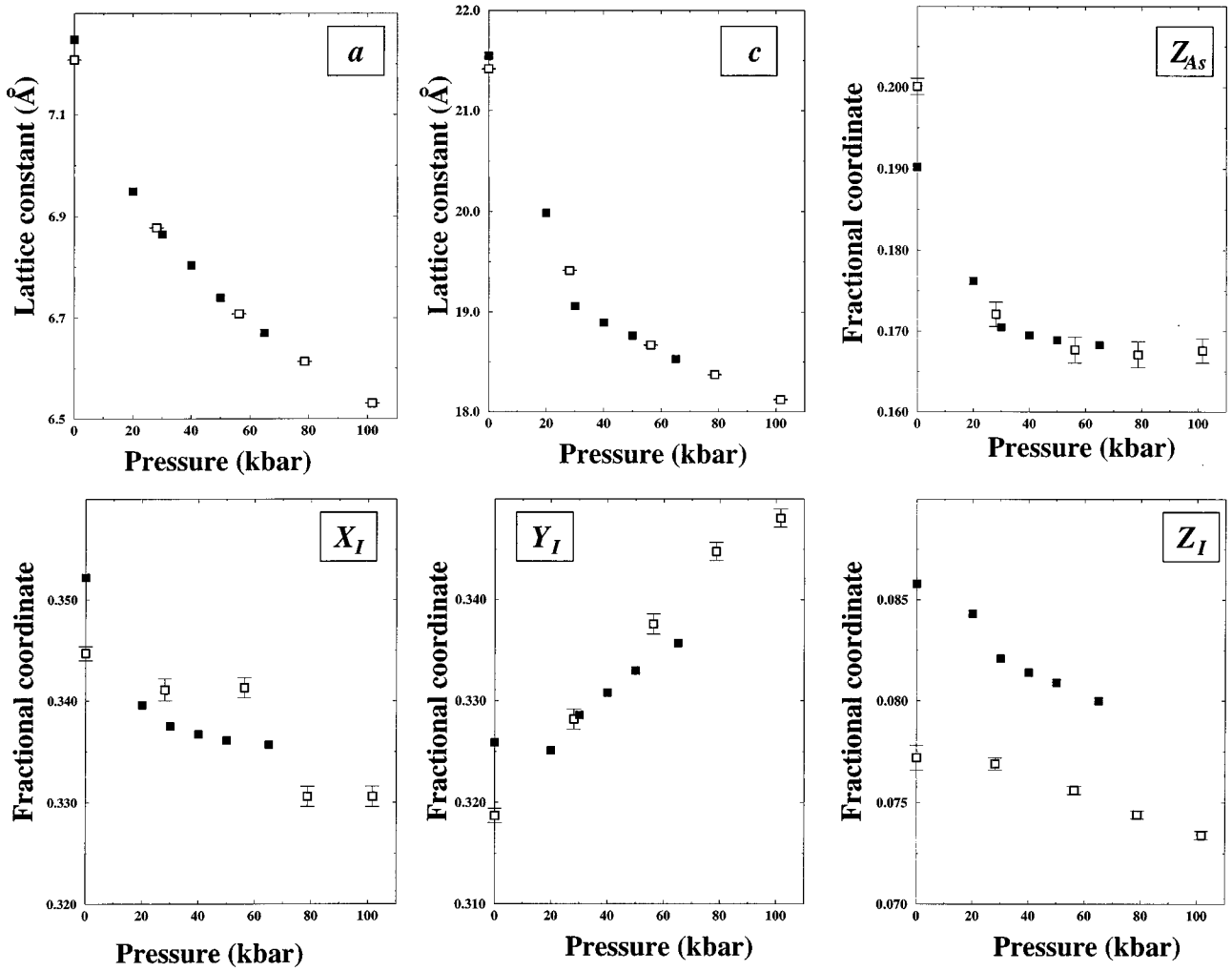

FIG. 6. The compression mechanism of the rhombohedral structure as obtained from experimental high-pressure angle dispersive powder x-ray diffraction (open squares) and by first-principles density functional simulations (filled squares).

moduli of the two phases are 1129.8 and 2262.6 kbar, respectively.

3. Kinetics and irreversibility

Decompression of the Bi compound results in a reversible transition as shown in Fig. 4(c). By contrast, the high-pressure modification of the Sb-compound was observed to persist down to ambient pressure at room temperature. The transition is therefore irreversible. As shown in Fig. 9 the density of this phase remains higher than that of the original ambient pressure phase. Other examples of irreversibility in pressure-induced structural phase transitions are known in the semiconductor-metallic transitions of the elemental semiconductors Si and Ge.[25] However, these transitions involve significant alterations of bond topology. The case of the triiodides appears to be somewhat different. Here there is only evidence of a weak first order transition between the rhombohedral and monoclinic phases as indicated from the volume change at the transition. And although the bonding is locally distorted, there is neither a topological change nor a coordination number change at the transition with both phases being approximately sixfold at the transition pressure. On these grounds, it is clear that bond topology is not responsible for the irreversibility of the transition. The origin of the irreversibility may be that while the different bonding configurations in the two phases appear to be favorable over a range of pressures, there must exist a kinetic barrier to continuous distortion from one to the other. We also expect that the observed irreversibility must require the energies of the high-pressure and ambient-pressure phases to be similar over a relatively wide range of densities. Both these scenarios could be explored in more detail through the use of first-principles simulations, however, we will not explore this further in the present paper.

TABLE III. Refined internal structural parameters in fractional coordinate for SbI_3 at 101 kbar.

Atom	*x*	*y*	*z*
Sb	0.0209(2)	−0.2078(3)	0.1113(3)
I_1	0.2335(2)	0.0734(1)	0.2065(5)
I_2	0.3689(1)	−0.2642(2)	0.4695(1)
I_3	−0.2017(4)	−0.0510(1)	0.3205(3)

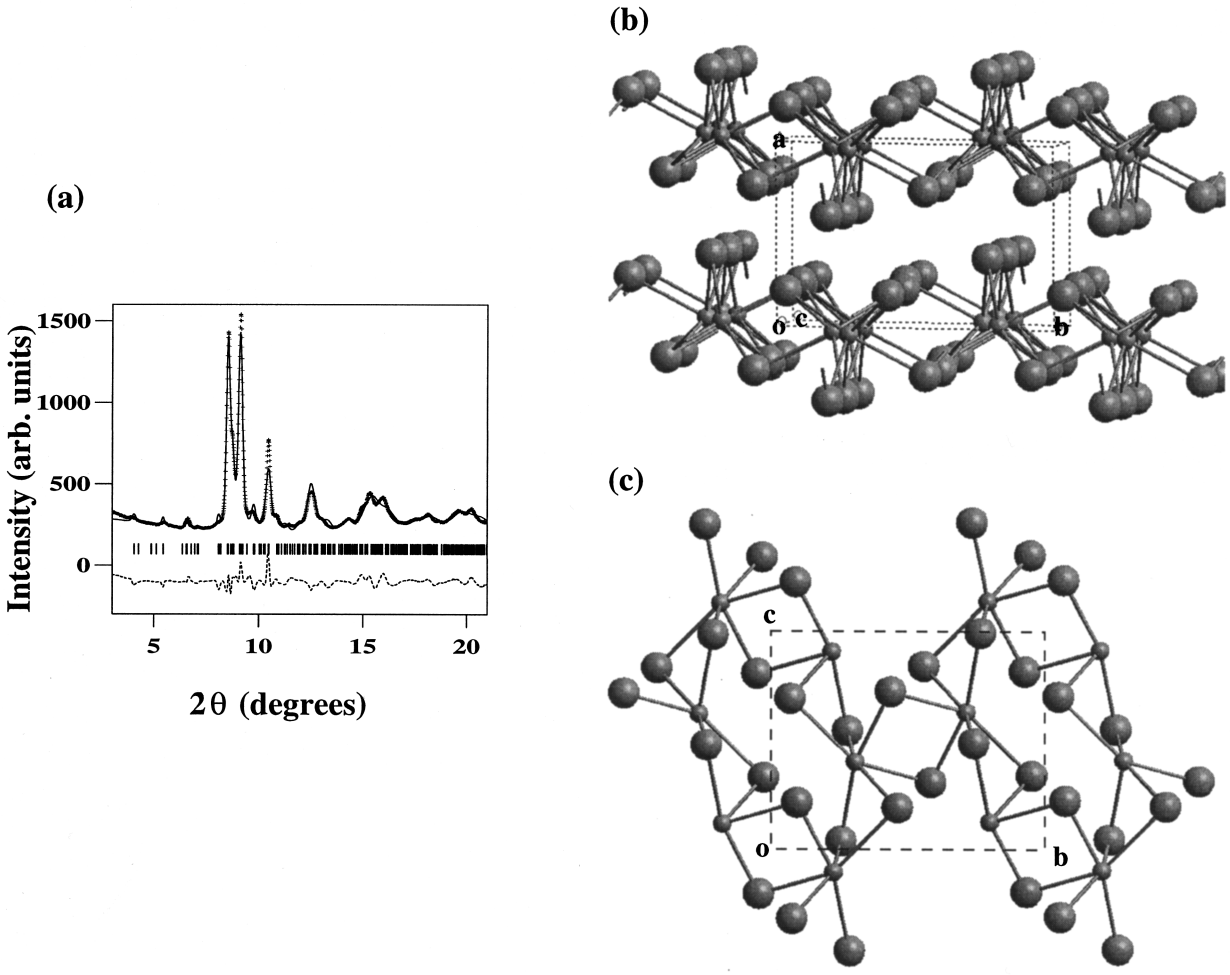

FIG. 7. Rietveld refinement of powder pattern of SbI_3 observed at 101 kbar (a). The fit shown in (a) has been obtained using a (l00) preferred orientation correction. The reliability factor $R_{wp}(\%)$ is 6.48. Illustration of the relevant puckered layered structure [having space group $C_{2h}^5(P2_1/c)$] along different view point is shown in (b) and (c). The small and large spheres stand for the Sb atoms and I atoms, respectively.

C. Ambient-pressure vibrational properties

The observed Raman mode frequencies of the group-V metal tri-iodides are shown in Table IV at 300 and 12 K at ambient pressure along with their symmetry labels and mode types. The spectra from which these results are obtained are shown in Fig. 10. In the case of As and Sb compounds there exist two low-frequency modes designated as translations. These refer to relative movements of the centers of mass of

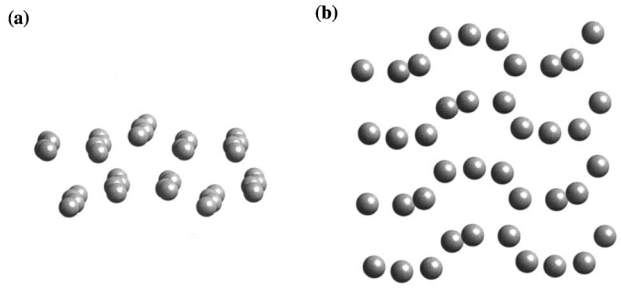

FIG. 8. The projection of Iodine sublattice parallel (a) and normal (b) to the buckled layers under high pressure shows the distortion induced by compression.

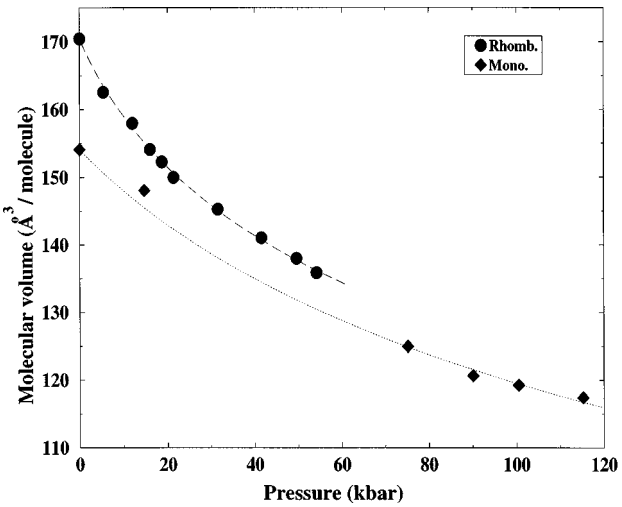

FIG. 9. Molecular volume vs pressure for SbI_3 illustrating the relatively small volume collapse and the irreversibility of the transition under decompression. The low-pressure phase (rhombohedral) is denoted as the solid circle whereas the high-pressure phase (monoclinic) is shown as the solid diamond. The dashed and dotted lines represent a fit to the Birch-Murnaghan equation of state.

TABLE IV. Observed Raman frequencies of three group-V metal tri-iodides at room and low temperature. The frequency is in units of cm^{-1}. The abbreviations *s*, *b*, *l*, and *t* refer to stretching, bending, librational, and translational modes. The translational mode refers to relative motion of the molecules in a unit cell and is therefore a type of lattice mode. RL stands for rigid layer.

Symmetry		AsI_3			SbI_3		BiI_3		Symmetry
Species	300 K	12 K	Calc.	300 K	12 K	300 K	12 K	Species (BiI_3)
$E_g(s)$	207.5	206.9	209.0[d]	160.6	159.1	115.5	114.7	A_g
	208.2[a]	206.5[b]	167.1[e]	161.5[a]	158.0[b]		113.3[c]	
$A_g(s)$	185.5	180.4	177.7[d]	138.3	134.7	87.4	94.4	E_g
	187.1[a]	180.0[b]	125.1[e]	139.0[a]	132.5[b]		95.0[c]	
$A_g(b)$	84.5	83.8	83.6[d]	66.9	67.5	56.3	58.0	A_g
	84.6[a]	83.5[b]	69.9[e]	73.0[a]	67.0[b]		58.5[c]	
$E_g(b)$	74.1	76.6	74.9[d]	74.2	79.8	52.8	53.7	A_g
	73.9[a]	76.5[b]	85.5[e]		81.0[b]		53.5[c]	
$E_g(l)$	62.0	64.1		60.8	62.2	34.6	34.8	E_g
		64.0[b]			62.0[b]		36.7[c]	
$A_g(t)$	57.3	61.2		46.0	47.6			E_g
	56.0[a]	61.0[b]		45.5[a]	47.5[b]		33.5[c]	
$A_g(l)$	39.5	43.1		38.5	40.1	22.4	22.6	$A_g(RL)$
	39.0[a]	43.0[b]		38.0[a]	40.0[b]		22.8[c]	
$E_g(t)$	34.3	37.3						$E_g(RL)$
	33.3[a]	37.5[b]		33[a]	35.5[b]		12.9[c]	

[a]Reference 26.
[b]Reference 27.
[c]Reference 28.
[d]GGA.
[e]LDA.

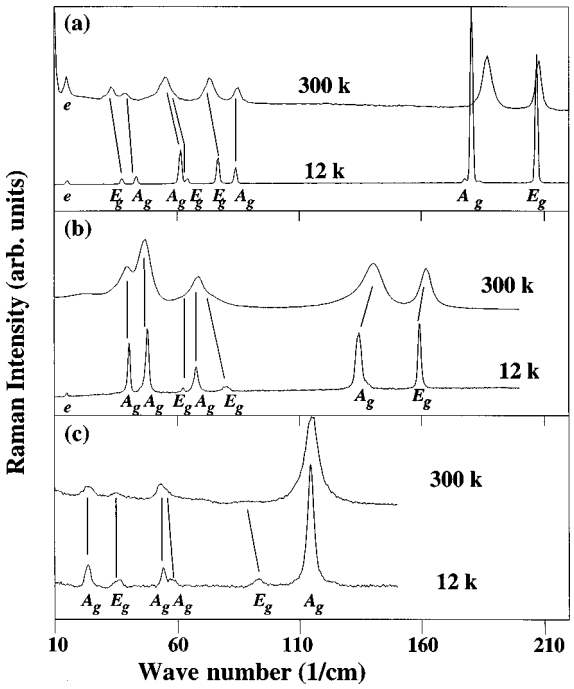

FIG. 10. Raman spectra at room (300 K) and low (12 K) temperature for AsI_3 (a), SbI_3 (b), and BiI_3 (c). The assignment derived from depolarization ratios (Refs. 27,28) is shown for the corresponding peak. The signal of emission line is denoted as *e*.

the two molecules in the unit cell and are therefore lattice modes by analogy with molecular crystals. In the Bi material, these modes are more similar to rigid layer modes in quasi-2D solids.

Our experimentally determined frequencies for the ambient pressure phase are clearly in good agreement with previous studies.[26–28] In this table we also show the results of our theoretical calculations again highlighting the differences between the LDA and GGA predictions for mode frequencies. In this case the LDA calculations give a lower value for the *X*-I stretch frequency than do the GGA results. This is consistent with the LDA calculation relating to an overly compressed structure. In this case the result of this is depletion of the bond charge from the original XI_3 molecules thereby reducing the bond strength and the associated stretch frequency.

D. Pressure-induced response of vibrations

1. High-frequency spectral region

The evolution of the Raman spectra for these three compounds are shown in Fig. 11. Application of pressure to the Sb and As compounds clearly gives rise to an initial softening of the symmetric stretch frequency in both cases which is indicative of a weakening of the intramolecular bond. Moreover, the mode-Grüneisen parameter γ_i for this pressure-induced softening A_g mode of AsI_3 and SbI_3 is -3.9 and -11.8, respectively (the corresponding γ_i for this symmetric

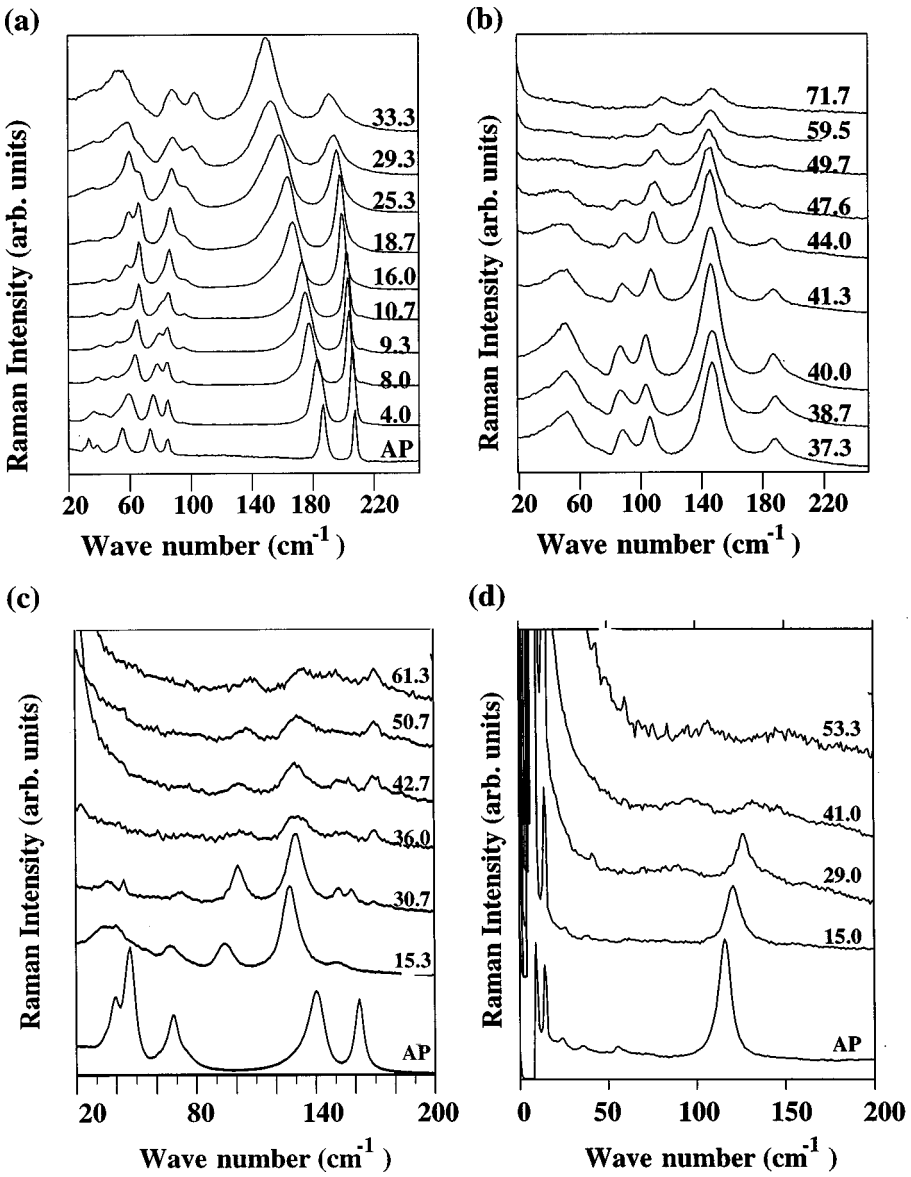

FIG. 11. Observed Raman spectrum of AsI_3 (a),(b), SbI_3 (c), and BiI_3 (d) as a function of pressure. The hydrostatic pressure for the corresponding spectrum is in a unit of kbar.

stretching A_g mode of BiI_3 is +3.7). This weakening is observed to saturate upon further compression and then to increase again giving rise to an unusual nonmonotonic pressure variation. We attribute this behavior to pressure-induced intramolecular to intermolecular bond charge transfer and the development of ionic bonding character. This leads simultaneously to the enhancement of intermolecular cohesion and weakening of the molecular units in Sb- and As-containing systems.

A calculation of the pressure dependence of the vibrational mode frequency corresponding to the symmetric *X*-I stretch has been performed for AsI_3 and the results are shown in Fig. 12. It is clear that the complex nonmonotonic pressure variation of this mode is well accounted for in the simulated data and that the pressure at which the frequency decrease levels off is similar in both the experimental and simulated situations. Despite rather good quantitative agreement between experimental and calculated frequencies, it is clear that the simulation underestimates the experimental values. The origin of this underestimate we attribute to the difference in temperature between the experimental and simulated systems. Specifically, the density functional simu-

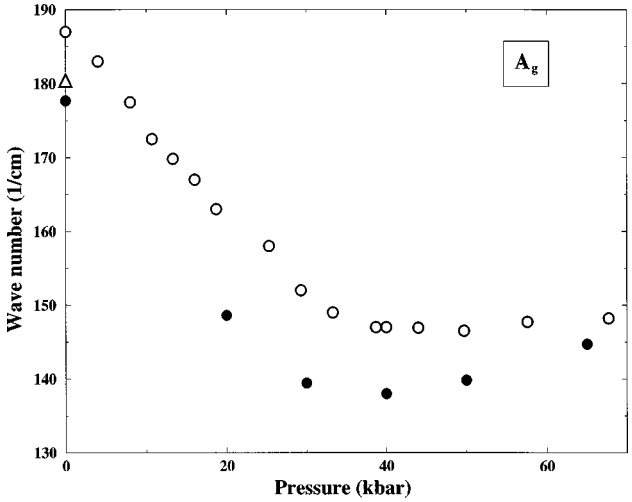

FIG. 12. The pressure variation of the *X*-I symmetric stretch vibrational mode for AsI_3 as obtained from Raman spectroscopic data (open circles) and from density functional calculations (filled circles) using full structural relaxation. The open triangle corresponds to the 12 K measurement at ambient pressure.

TABLE V. Comparison between observed room-temperature intramolecular modes at 18.7 kbar and corresponding frequencies generated from GGA calculations at 20 kbar.

Symmetry species	Exp. (18.7 kbar)	GGA calc. (20 kbar)
$E_g(s)$	198.5	194.8
$A_g(s)$	163.5	148.6
$A_g(b)$	86.0	78.9
$E_g(b)$	93.0	86.5

lation is performed at $T=0$ whereas the pressure measurements are performed at ambient temperature. The implication is clear from the low-temperature data presented in Fig. 10 and Table IV where the X-I stretch frequency is found to decrease with decreasing temperature and this accounts for much of the small (<10 cm^{-1}) difference between measurement and theory. The effect of temperature on the mode frequencies is also likely to be the origin of the underestimate of the bulk modulus for AsI_3 obtained in the calculations. Also, we note that the calculation predicts slightly more pronounced recovery of the bond strength than does the experimental observation and we expect that this would be observable at lower temperatures.

It is clear that incorporation of gradient corrections correctly accounts for the initial softening with pressure of the E_g intramolecular stretching mode. Quantitative agreement with experiment is also good with both suggesting a $\approx 6\%$ drop over 20 kbar. The results of the GGA calculation of intramolecular modes at a pressure of 20 kbar are shown in Table V as are the experimental results at a pressure of 18.7 kbar.

In view of this high-pressure data we are in a position to comment further on the underestimate of the calculated *ambient* pressure zone center phonon frequencies using the local density approximation. Specifically, it is clear that LDA calculation of the stretch frequency is far too low and cannot be associated with a realistic effective pressure. Instead, it appears that neglect of gradient corrections (i.e., use of the LDA level of approximation) leads to an intramolecular bond which is too weak and an intermolecular bond which is too strong.

2. Low-frequency spectral region

Figure 13(a) shows the evolution with pressure of the low-frequency region of the Raman spectrum of AsI_3 from ambient to 33.3 kbar and over the range 30 to 75 cm^{-1}. At ambient pressure, the molecular libration mode [$A_g(l)$] and the molecular translation mode [$A_g(t)$] having the same symmetry are located at 39.5 and 57.3 cm^{-1}, respectively. Moreover, as shown in Fig. 13(b), the separation between the $A_g(t)$ and $A_g(l)$ modes decreases from 17.8 to 6 cm^{-1} under compression of the AsI_3 sample up to 18.7 kbar. This implies the presence of disparate pressure coefficients for the two vibrational modes. Increasing pressure to about 26 kbar, two external modes are still not overlapping and the frequency separation remains almost constant. However, the Raman intensity of the $A_g(t)$ mode transfers gradually to the one of the $A_g(l)$ modes within this pressure range [shown in Fig. 13(a)]. At higher pressures, the frequency discrepancy increases slightly and the intensity transfer procedure is nearly complete at 33.3 kbar.

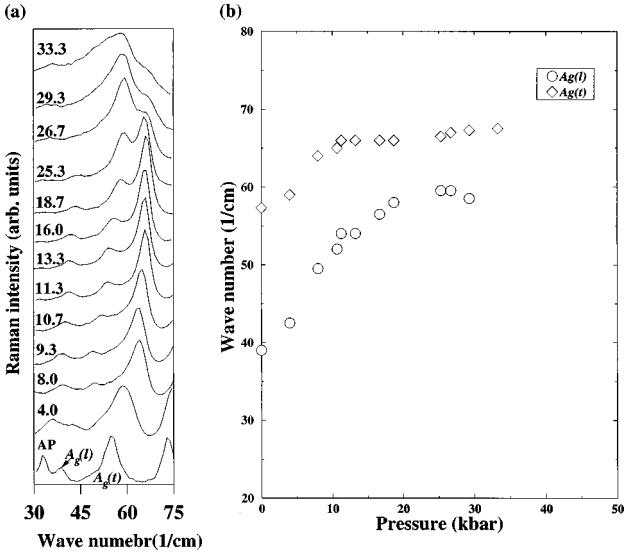

FIG. 13. (a) Observed Raman spectrum of AsI_3 as a function of pressure within low-frequency region. (b) Variation of the molecular libration $A_g(l)$ frequency and the molecular translation $A_g(t)$ frequency with pressure.

Such behavior of the Raman shifts and intensities is attributed to *Fermi resonance* which refers to the quantum-mechanical mixing of two vibrational modes with identical symmetry under an anharmonic intermolecular coupling potential.[29] This pressure-tuned Fermi resonance has also been observed in other molecular systems (such as $KBr/CaSO_4$,[30] liquid ethylene carbonate,[31] and ice[32]) which correspond to the coupling between a normal mode and an overtone. Nevertheless, in the case of quasimolecular AsI_3, this resonance is formed by the mixing of the libration and the translation of the molecular unit. Based on perturbation theory,[31] the intermolecular dipole moment coupling constant as a function of pressure can be quantitatively derived from the accurate Raman intensity ratio of two resonance bands. Therefore, in order to obtain the anharmonic coupling constant of AsI_3, more measurements of Raman frequencies and intensities are needed.

IV. DISCUSSION AND CONCLUSIONS

The effect of high pressure on a crystallographically isostructural family of molecular solids have revealed considerable complexity in their response to compression which is reflected in their electronic properties, crystal structure and dynamic behavior. In particular, the high-pressure phases are found to be of very low symmetry having highly distorted quasi-sixfold coordinated bonding but the reconversion to the stable ambient pressure phase appears to be hindered by barriers to distortion of this bonding configuration resulting in transition barriers and irreversibility which are strongly dependent on the chemical nature of the metal species. Vibrational properties illustrate that the effect of pressure is to reduce anisotropy of the cohesive forces by enhancing inter-

molecular bonds at the expense of intramolecular forces. The application of first principles computer simulation has been effective in accounting for the pressure effects on the structural, electronic, and dynamical properties. However, it is found that the commonly used LDA is not appropriate for this system and that the errors incurred are not attributable to an effective pressure.

ACKNOWLEDGMENTS

J.C. would like to thank the EPCC in Edinburgh for the T3D resources. J.C. wishes also to thank the Royal Society of Edinburgh for support. H.C.H. also acknowledges computer time at the National Center for High-performance Computing which was provided by National Science Council, Taiwan, R.O.C. Grant No. NSC 87-2112-M-032-013.

[1] J. M. Besson, J. Cernogora, and R. Zallen, Phys. Rev. B **22**, 3866 (1980).
[2] B. A. Weinstein and R. Zallen, *Light Scattering in Solids IV*, edited by M. Cardona and G. Güntherodt (Springer-Verlag, Berlin, 1984), p. 463.
[3] H. C. Hsueh, Ph.D. thesis, University of Edinburgh, 1997.
[4] R. O. Piltz, M. I. McMahon, J. Crain, P. D. Hatton, R. J. Nelmes, R. J. Cernik, and G. Bushnell-Wye, Rev. Sci. Instrum. **63**, 700 (1992).
[5] H. C. Hsueh, H. Vass, S. J. Clark, and J. Crain, Europhys. Lett. **31**, 151 (1995).
[6] M. C. Payne, M. P. Teter, D. C. Allan, T. A. Arias, and J. D. Joannopoulos, Rev. Mod. Phys. **64**, 1046 (1992).
[7] H. C. Hsueh, M. C. Warren, H. Vass, G. J. Ackland, S. J. Clark, and J. Crain, Phys. Rev. B **53**, 14 806 (1996).
[8] H. C. Hsueh, H. Vass, S. J. Clark, G. J. Ackland, and J. Crain, Phys. Rev. B **51**, 16 750 (1995).
[9] H. C. Hsueh, W. C. K. Poon, H. Vass, and J. Crain, Europhys. Lett. **35**, 689 (1996).
[10] W. Kohn and L. J. Sham, Phys. Rev. **140**, A1133 (1965).
[11] R. P. Feynman, Phys. Rev. **56**, 340 (1939).
[12] J. S. Lin, A. Qteish, M. C. Payne, and V. Heine, Phys. Rev. B **47**, 4174 (1993).
[13] M. H. Lee, Ph.D. thesis, University of Cambridge, 1995.
[14] H. J. Monkhorst and J. D. Pack, Phys. Rev. B **13**, 5188 (1976).
[15] J. P. Perdew and A. Zunger, Phys. Rev. B **23**, 5048 (1981).
[16] J. P. Perdew, J. A. Chevary, S. H. Vosko, K. A. Jackson, M. R. Pederson, D. J. Singh, and C. Fiolhais, Phys. Rev. B **46**, 6671 (1992).
[17] H. C. Hsueh, H. Vass, F. N. Pu, S. J. Clark, W. C. Poon, and J. Crain, Europhys. Lett. **38**, 107 (1997).
[18] J. Trotter and T. Zobel, Z. Kristallogr. **123**, 67 (1966).
[19] R. Enjalbert and J. Galy, Acta Crystallogr., Sect. B: Struct. Crystallogr. Cryst. Chem. **36**, 914 (1980).
[20] R. O. Jones and O. Gunnarsson, Rev. Mod. Phys. **61**, 689 (1989).
[21] H. Akbarzadeh, S. J. Clark, and G. J. Ackland, J. Phys.: Condens. Matter **5**, 8065 (1993).
[22] G. Kresse, J. Furthmuller, and J. Hafner, Phys. Rev. B **50**, 13 181 (1994).
[23] S. Pohl and W. Saak, Z. Kristallogr. **169**, 177 (1984).
[24] A. S. Miguel, A. Polian, and J. P. Itie, J. Phys. Chem. Solids **56**, 555 (1995).
[25] J. Crain, G. J. Ackland, and S. J. Clark, Rep. Prog. Phys. **58**, 705 (1995).
[26] W. Kiefer, R. G. Humphreys, and M. Cardona, Z. Naturforsch. A **25A**, 1101 (1970).
[27] A. Anderson, J. A. Campbell, and R. W. G. Syme, J. Raman Spectrosc. **19**, 379 (1988).
[28] T. Komatsu, T. Karasawa, T. Iida, K. Miyata, and Y. Kaifu, J. Lumin. **24/25**, 679 (1981).
[29] F. Rasetti, Nature (London) **123**, 205 (1929).
[30] S. Lewis and W. F. Sherman, Spectrochim. Acta A **35**, 613 (1979).
[31] W. Schindler, T. W. Zerda, and J. Jonas, J. Chem. Phys. **81**, 4306 (1984).
[32] K. Aoki, H. Yamawaki, and M. Sakashita, Science **268**, 4306 (1995).